Experimental assessment of energy consumption: a comparative study between motor-controlled and valve-controlled cylinders in knuckle boom crane operations

Wei Zhao[1]*, Morten Kjeld Ebbesen[1], Michael Rygaard Hansen[1] and Torben Ole Andersen[2]

[1]Department of Engineering Sciences, University of Agder, Kristiansand, Norway, [2]Department of Energy Technology, Aalborg University, Aalborg, Denmark

This paper experimentally assess the energy consumption of a laboratory knuckle boom crane utilizing two proposed two-motor-two-pump (2M2P) motor-controlled hydraulic cylinders (MCC) in comparison to two conventional valve-controlled hydraulic cylinders (VCC). Experimental results demonstrate that using the motor-controlled crane instead of the valve-controlled crane results in 60%–64% total energy savings. In conclusion, this study highlights the practical suitability of the 2M2P MCCs for real-world applications, showcasing their enhanced energy efficiency compared to conventional VCCs.

1 Introduction

Hydraulic cylinders are widely used in heavy-duty industries due to their inherent advantages, such as high power density, ability to withstand shock loads, and reliability in harsh operational conditions. In the past years, the valve-controlled hydraulic cylinder (VCC) circuits have been the standard and dominating the market. While VCCs are known for their simplicity, robustness, and mature technology, their energy efficiency is limited by throttling losses inherent in both the control and counterbalance valves. For instance, the efficiency of valve-controlled hydraulic cranes typically ranges from 8.5% for conventional systems to 27.3% for load-sensing valve-controlled systems (Liang et al., 1999). In excavators equipped with valve-controlled hydraulic systems, approximately 35% of the total input energy is consumed by the control valves (Zimmerman et al., 2007).

Given the ongoing climate crisis, there is a growing recognition of the critical role energy efficiency plays. Various strategies to enhance the energy efficiency of valve-controlled hydraulic cylinder systems can be broadly categorized into two approaches: cylinder-side methods and control system side methods. Cylinder-side methods primarily focus on reducing the weight of hydraulic components by utilizing lightweight yet strong materials Lubecki et al. (2022). However, these solutions are predominantly suited for mobile applications. On the control system side, transitioning toward valve-less control
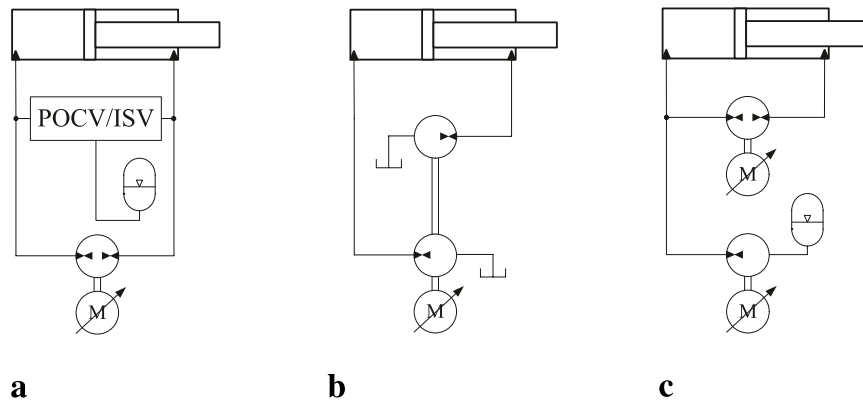
FIGURE 1
Main MCC topologies (Zhao et al., 2022). **(A)** 1M1P MCC. **(B)** 1M2P MCC. **(C)** 2M2P MCC.

systems has emerged as a promising approach to minimize valve throttling losses and significantly improve efficiency across a wider range of applications. This transition can be achieved by using a motor-controlled hydraulic cylinder (MCC), where a hydraulic cylinder is directly connected to fixed-displacement hydraulic pump(s) driven by electric servo motor(s). MCC enables manipulation of the hydraulic cylinder's motion by controlling the angular velocity(s) of the electric servo motor(s). MCCs can be classified into different configurations depending on the number of electric servo motors and hydraulic pumps utilized (Zhao et al., 2022). The main configurations comprise one-motor-one-pump (1M1P), one-motor-two-pump (1M2P), and two-motor-two-pump (2M2P) MCCs, as depicted in Figure 1. The abbreviations, POCV and ISV, are pilot-operated check valve and inverse shuttle valve, respectively. Most MCCs are equipped with a hydro-pneumatic accumulator serving as a low-pressure reservoir. While such accumulators help reduce excess pressure in the hydraulic system, alleviate transients, and improve system energy efficiency Lubecki et al. (2022), their contribution is inherently limited. This limitation arises because the accumulator pressure cannot exceed the hydraulic pump housing pressure, thereby restricting its impact on the overall energy efficiency of MCCs.

Incorporating MCCs into applications at system level, particularly in cases involving multiple cylinders, is important for the energy efficiency. Notably, the deployment of three 1M1P MCCs on an industrial pipe-racking crane yielded a remarkable 83.4% reduction in energy consumption compared to the conventional valve-controlled system (Hagen et al., 2019b). The incorporation of six 1M1P MCCs into an excavator yielded energy savings of 47.8% compared to excavators equipped with VCCs (Ahn et al., 2011). Despite the good energy-saving performance of the 1M1P MCC, it requires a mechanism of two POCVs or an ISV, as illustrated in Figure 1A, to compensate for differential flow rates. However, this mechanism may induce system oscillations under specific operational conditions (Williamson and Ivantysynova, 2008). Furthermore, conventional 1M1P MCCs lack the capability to achieve system pressure control and an energy-efficient load-holding function to manage hose rupture situations.

The 1M2P MCC configuration, depicted in Figure 1B, eliminates the need for a flow rate compensation mechanism. Additionally, it
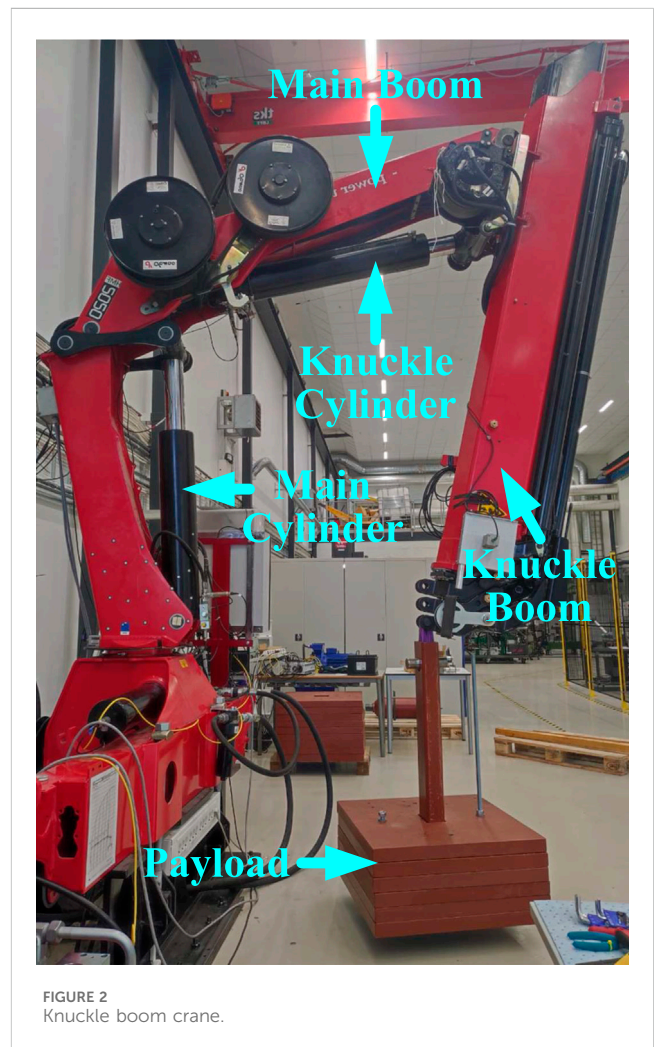

FIGURE 2
Knuckle boom crane.

demonstrates good energy efficiency performance compared to VCCs. For instance, according to the study in Zhang et al. (2017), an excavator powered by three 1M2P MCCs achieved a system efficiency of 73.3% within a given working cycle. However, the universal applicability of the 1M2P MCC is constrained by the
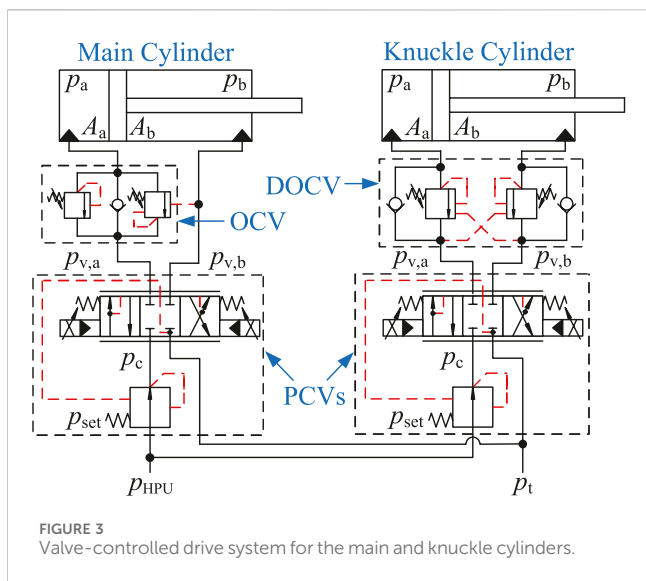
requirement that the displacement ratio of the two pumps must align with the ratio of cylinder areas. It is important to note that an efficient method for implementing a passive load-holding function to address hose rupture situations in 1M2P MCCs has not yet been established.

The 2M2P MCC, as depicted in Figure 1C, eliminates the need for a mechanism to compensate for the cylinder differential flow rate. Moreover, unlike the 1M2P MCC, the 2M2P MCC does not require precise alignment between the pump displacement ratio and the cylinder area ratio. This system is also capable of maintaining accurate system pressure control and enabling an energy-efficient passive load-holding function, even in the event of a power failure (Ketelsen et al., 2020). Furthermore, the 2M2P MCC offers the advantages of cylinder velocity being insensitive to load pressure changes and the capability to amplify load pressure through pump revolution (Cho and Helduser, 2008). Despite these numerous advantages, the 2M2P MCC needs to demonstrate superior energy performance compared to the market-dominating VCC to achieve widespread industrial implementation. However, a comprehensive comparison of their energy efficiencies, particularly in multi-cylinder systems, has yet to be conducted.

This paper aims to fill the existing gap by conducting an experimental comparison of the energy efficiencies between a two-cylinder knuckle boom crane driven by 2M2P MCCs and VCCs under two distinct load cases.

2 Systems in experiments

2.1 Knuckle boom crane

The knuckle boom crane used in this study is shown in Figure 2. It is an HMF model 2020-K crane, situated within the laboratory facilities at the University of Agder. This crane is equipped with five hydraulic actuators originally driven by valve-controlled drives. However, for the purpose of this study, only the main and knuckle cylinders are considered. They are responsible for driving the crane arms in the plane of the crane.

The main boom of the crane has a length of 2,400 mm and a mass of 206.5 kg, while the knuckle boom measures 2,430 mm in length and has a mass of 841.4 kg. Both the main and knuckle cylinders feature identical rod diameters of 100 mm. However, they are distinguished by different bore diameters, with the main cylinder having a bore diameter of 160 mm, whereas the knuckle cylinder has a bore diameter of 150 mm. Additionally, the main cylinder has a stroke of 750 mm, while the knuckle cylinder has a stroke of 852.5 mm.

2.2 Valve-controlled cylinder drive

The valve-controlled drive circuits for the main and knuckle cylinders are shown in Figure 3. The constant high-pressure source (p_{HPU} = 150 bar) and the low-pressure source (p_t = 0 bar) are supplied by the laboratory's ring line system. Within the drive circuits, two load-sensing proportional control valves (PCVs) are utilized. Both valves are mounted within a PVG32 valve block from Danfoss. Additionally, the main cylinder circuit incorporates an overcenter valve (OCV) from NEM where the relief functionality and the assistive load handling have been split into two parallel valves, while the knuckle cylinder circuit integrates a conventional double overcenter valve (DOCV) from Oil-Control. The pressure transducer used in the valve-controlled cylinder drive is from Rexroth, with the model number HM 20-2X/250-C-K35-N. The position transducer is a draw wire transducer from SELESCO, with the model number SP3-50. The controller used is a cRIO-9065 from National Instruments, with a sampling time of 0.01 s.

2.3 Proposed motor-controlled cylinder drive

Figure 4A shows the hydraulic diagram of the proposed 2M2P MCC. This design is consistent with the 2M2P MCC used in a previous study (Zhao et al., 2023). The system consists of two fixed-displacement pump/motor units known as the main unit (P_1) and the secondary unit (P_2). These units are driven by separate electric servo drives, designated as the primary electric servo motor/generator unit (M_1) and the secondary electric servo motor/generator unit (M_2). Notably, both M_1 and M_2 function as the control elements within the system.

The system inputs consist of velocity inputs of M_1 and M_2, denoted as $\omega_{1,input}$ and $\omega_{2,input}$, while ω_1 and ω_2 represent the velocities of the shafts. A low-pressure accumulator (ACC) functions as the pressurized reservoir, maintaining an approximately constant pressure of p_{acc} = 3 bar to supply the volumetric difference between the cylinder's rod side and bore side, as well as to the pumps during suction to prevent cavitation. The external leakage lines of the pumps are connected to the ACC via two check valves, CV6 and CV7. Additionally, two 2/2 normally closed load-holding valves, LHa and LHb, are controlled by the minimum cylinder pressure signal (p_{pi}), with a cracking pressure set at 10 bar.

Integrating load-holding valves into the cylinder's inlet and outlet is crucial in applications involving overrunning external loads to prevent load drop during critical situations such as power blackouts and hose ruptures. The p_{pi} signal is determined by the ISV, which switches its direction based on the bore-side pump pressure p_{pa} and the rod-side
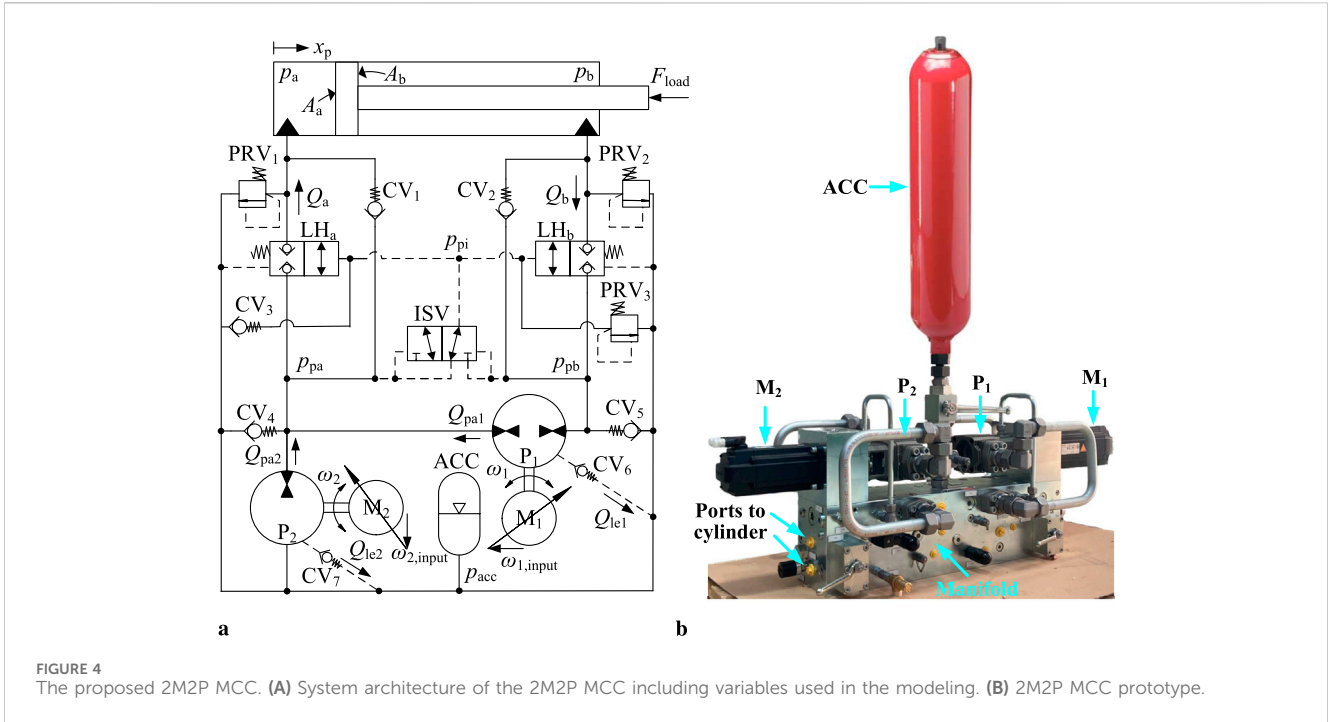
FIGURE 4
The proposed 2M2P MCC. **(A)** System architecture of the 2M2P MCC including variables used in the modeling. **(B)** 2M2P MCC prototype.

TABLE 1 Major components in 2M2P MCC.

Component	Manufacturer	Specifications
Electric Servo Motor$_1$	Bosch rexroth	T_{max} = 16.3 Nm, N_{max} = 2000 rpm
Electric Servo Motor$_2$	Bosch rexroth	T_{max} = 7.2 Nm, N_{max} = 2,990 rpm
Axial Piston Pump$_1$	Bosch rexroth	D_p = 6 cc/rev
Axial Piston Pump$_2$	Bosch rexroth	D_p = 3 cc/rev
Shuttle valve	Bucher hydraulics	p_{max} = 350 bar, Q_{max} = 16 L/min
Load Holding Valve	Sun hydraulics	p_{max} = 345 bar, Q_{max} = 227 L/min, p_{pilot} = 10 bar
Check Valve	Bosch rexroth	p_{max} = 420 bar, Q_{max} = 120 L/min, p_{crack} = 0.2 bar
Pressure Relief Valve	Bosch rexroth	Q_{max} = 50 L/min, p_{max} = 400 bar, p_{crack} = 200 or 80 bar
PLC	Bosch rexroth	RAM 512 Mb, Sercos

pump pressure p_{pb}. The role of the ISV is to ensure that the controlled lowest cylinder pressure is consistently fed to the load-holding valves. To improve system response, two check valves (CV$_1$ and CV$_2$) are installed in parallel with the load-holding valves. Moreover, three pressure relief valves (PRV$_1$, PRV$_2$, and PRV$_3$) are integrated to prevent system overpressure, while three check valves (CV$_3$, CV$_4$, and CV$_5$) sustain line pressures higher than p_{acc}. The proposed 2M2P MCC operates in two distinct modes: the operation mode and the load-holding mode. During the operation mode, the p_{pi} pressure is regulated to be higher than 10 bar, opening LH$_a$ and LH$_b$, thereby allowing the piston position (x_p) to adjust based on the command signal. Conversely, in the load-holding mode, p_{pi} is controlled to be lower than 10 bar, causing LH$_a$ and LH$_b$ to close, maintaining the cylinder piston in a stationary position.

The prototype of the proposed 2M2P MCC is shown in Figure 4B. The major components used in the 2M2P MCC

prototype, along with their respective parameters as provided by the manufacturers are listed in Table 1. The pressure and position transducers used in the motor-controlled cylinder drive are identical to those used in the valve-controlled cylinder drive. The angular velocities and torques of M$_1$ and M$_2$ are measured by two Rexroth IndraDrive HMS01 units. The controller used is Bosch Rexroth's IndraControl XM21/22, with a sampling time of 0.002 s.

3 Control algorithm

3.1 VCC control algorithm

Given the primary objective of this paper, which is to identify the differences in the energy efficiency performance between two different drive systems, further development of the control
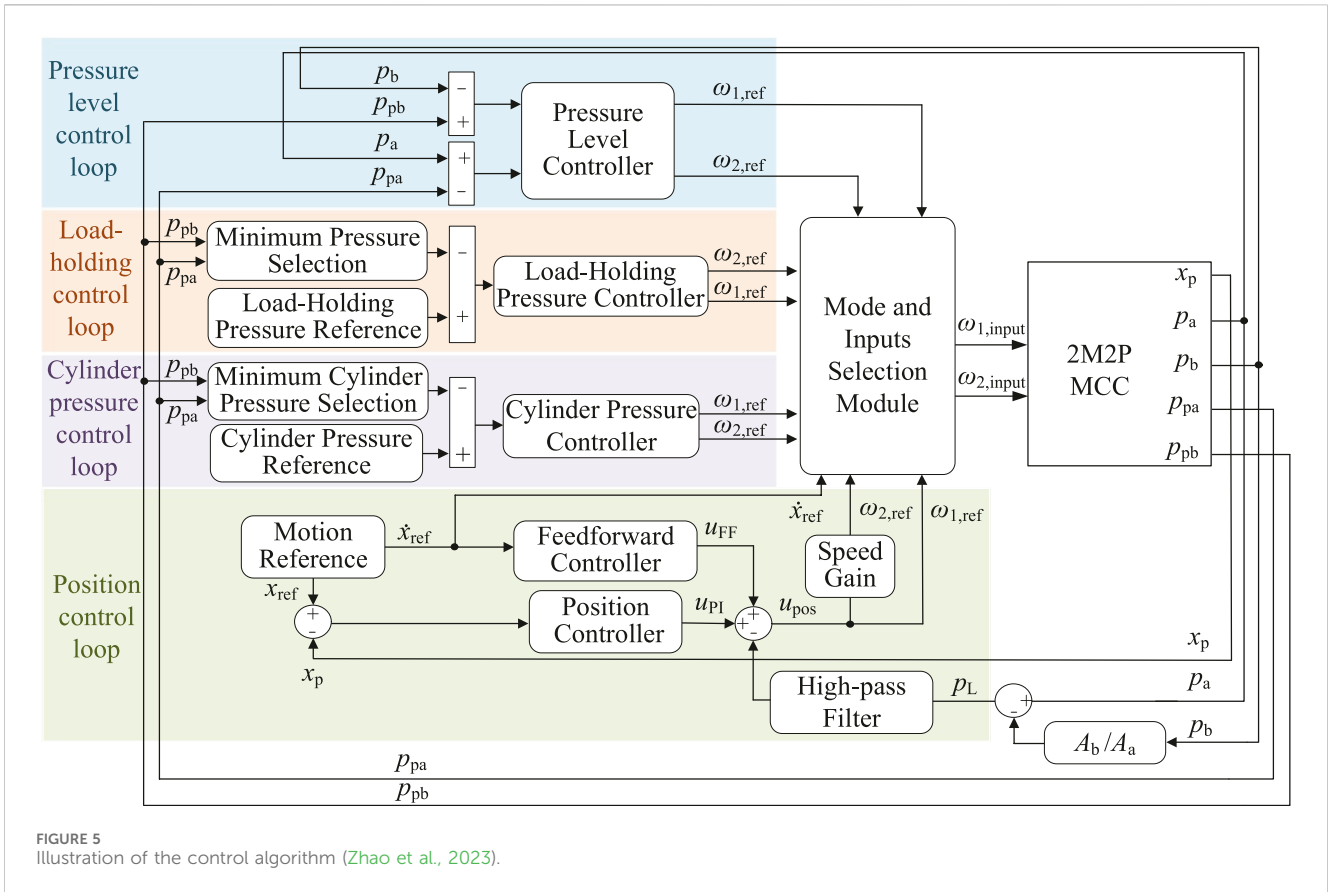
FIGURE 5
Illustration of the control algorithm (Zhao et al., 2023).

algorithm for the VCCs is not pursued. Instead, two Proportional-Integral (PI) controllers are employed to ensure the main and knuckle cylinders track the position reference signals reasonably accurate. The main cylinder's PI controller is configured with a proportional gain of 4,000 m^{-1} and an integral gain of 400 $m^{-1}s^{-1}$, while the knuckle cylinder's PI controller utilizes a proportional gain of 3,000 m^{-1} and an integral gain of 300 $m^{-1}s^{-1}$.

3.2 MCC control algorithm

The control algorithm, originally proposed for 2M2P MCCs in Zhao et al. (2023), is utilized in this study. Illustrated in Figure 5, this algorithm comprises four different control loops: the position control loop, cylinder pressure control loop, load-holding control loop, and pressure level control loop. Outputs from these loops are strategically selected by the mode and inputs selection module and subsequently integrated into the system. This approach ensures the realization of four-quadrant operation, passive load-holding functionality, and seamless transitions between these operational states. A comprehensive explanation of this control algorithm is available in (Zhao et al., 2023). Following verification via the simulation model, the control algorithm is implemented and tuned on the experimental setup. The PI controller gains in the four control loops are provided in Table 2. The cylinder pressure reference is set to 15 bar because the cracking pressure of valves LH_a and LH_b is 10 bar. After considering a safety margin to account for potential variations and ensure system stability, a pressure level of

TABLE 2 Controller gains in the MCC control algorithm.

Controllers	P	I
Position controller	30 rev/min/m	5 rev/min/m/s
Cylinder pressure controller	20 rev/min/bar	5 rev/min/bar/s
Load-holding controller	20 rev/min/bar	4 rev/min/bar/s
Pressure level controller	50 rev/min/bar (bore side)	0 rev/bar (bore side)
Pressure level controller	10 rev/min/bar (rod side)	0 rev/bar (rod side)

15 bar was selected. The load-holding pressure reference is set to 3 bar.

4 Experiment and results

4.1 Generated crane lifting path

The crane path, depicted by the red trajectory in Figure 6, is designed to facilitate the movement of the crane while lifting a payload within the specified operational range outlined by the blue line. This path is carefully crafted, taking into account the constraints of the laboratory crane without triggering the saturation of M_1 and M_2. During experiments, both the valve-controlled and motor-controlled cranes are tasked with following this predefined path while lifting payloads in two load cases: 0 and
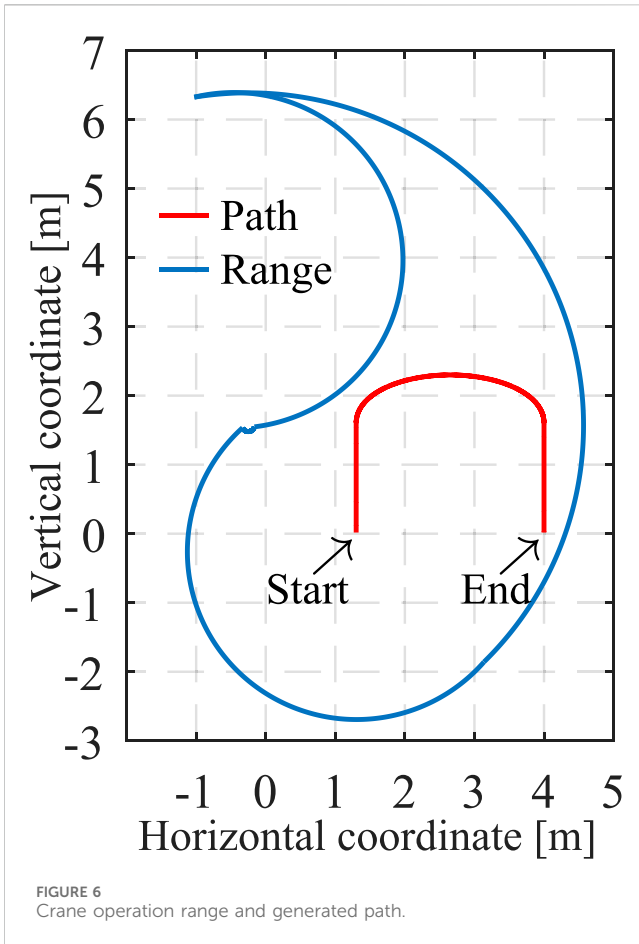
FIGURE 6
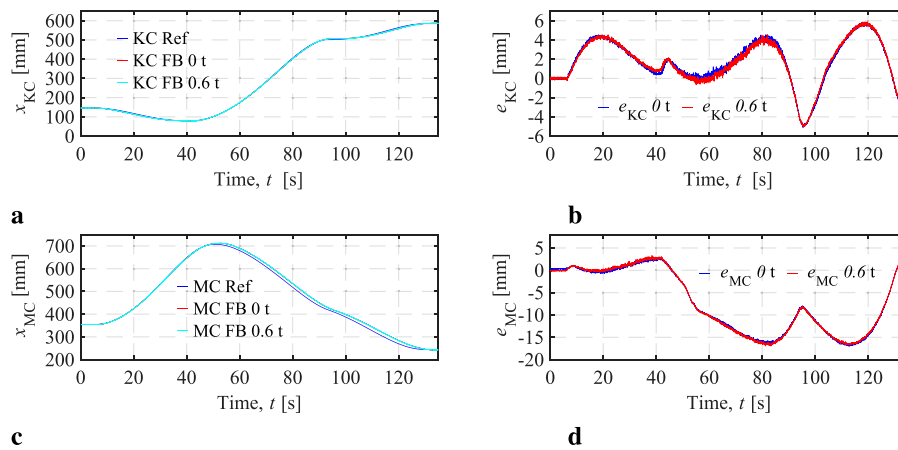Crane operation range and generated path.

follow the position references, with minimal deviation, as shown in Figures 7B, D. Notably, the tracking errors remain within acceptable limits across the two load cases. The knuckle cylinder exhibits tracking errors well within ±6 mm, while the main cylinder's tracking error increases slightly from ±3 mm to ±17 mm during retraction.

It should be noted that the primary focus of this study is the comparison of energy performance, and therefore, advanced control algorithms for the VCCs were not investigated or applied. Despite this, the position tracking performance of the valve-controlled knuckle boom crane is considered acceptable for the purpose of assessing energy efficiency. However, the tracking errors observed could potentially be reduced with further effort on controller optimization.

The pressures of the knuckle and main cylinders in the valve-controlled crane are illustrated in Figure 8. The rod-side pressure is denoted as p_b for both the knuckle and main cylinders, while the bore-side pressure is represented as p_a for both cylinders. It can be observed that when the cylinders change direction (during the transition period between different quadrants), the pressures on the rod side and bore side of the cylinders experience sudden changes and intersect each other. In the experiments, the main cylinder operates in the first and fourth quadrants. Consequently, its bore-side pressure (p_a) typically exceeds the rod-side pressure (p_b), except during the transition periods. Furthermore, the main cylinder bore-side pressure increases as the load increases.

In the experiments, as the crane follows an open path, the knuckle cylinder operates through the third, second, and first quadrants, exhibiting more complex pressure variations than the main cylinder. Notably, with a 0.6 t payload, the knuckle cylinder pressures intersect during directional changes, with the bore-side pressure consistently surpassing the rod-side pressure after the intersection. On the other hand, under a 0 t payload, there is no intersection; the rod-side pressure remains higher than the bore-side pressure. This occurs because the 0 t payload is insufficient to cause p_a to exceed p_b during knuckle cylinder extension.

The hydraulic power and cylinder mechanical power, along with the energy efficiencies of the two cylinders in the valve-controlled crane, are depicted in Figure 9. The cylinder mechanical power in VCCs, denoted as P_C, is calculated using Equation 1. In this calculation, v represents the cylinder velocity, which is derived and filtered from the experimental data, while F_{cyl} represents the hydraulic force generate by the cylinder. The force F_{cyl} is calculated using Equation 2, where A_a and A_b are the bore-side and rod-side areas of the cylinder, respectively. The cylinder friction force is not included in the mechanical power calculations for both valve-controlled and motor-controlled cranes because it cannot be directly measured during the experimental tests. However, the friction losses are identical for both systems since they follow the same crane lifting path. The hydraulic input power in VCCs, denoted as P_H, is calculated using Equation 3. Here, p_{HPU} represents the pressure of the laboratory hydraulic power unit (HPU), while Q_{in} represents the flow rate from the HPU to the cylinder. Since the pressure relief valves are never activated, the Q_{in} is approximately calculated by Equation 4. The p_{HPU} is set to 150 bar, being the minimum pressure to drive the crane with the 0.6 t payload.

0.6 t. A comparison of the efficiencies inherent to the two drive systems is conducted across these load cases.

It is important to note that the knuckle boom crane was originally equipped with a valve-controlled drive system for both the main and knuckle cylinders. The 2M2P MCC prototype was utilized for both the main and knuckle cylinders, but not simultaneously, as only one prototype was available. For each load case, the crane was operated twice: first, with the prototype connected to the main cylinder while the valve-controlled system operated the knuckle cylinder, and second, with the prototype connected to the knuckle cylinder while the valve-controlled system operated the main cylinder. This approach ensured comprehensive testing of both configurations.

4.2 Valve-controlled crane

The position tracking performances of the two cylinders in the valve-controlled knuckle boom crane, across two load cases, are depicted in Figure 7. The reference signals for both the main and knuckle cylinders (denoted as "Ref" in the figures) are derived from inverse kinematic calculations based on the provided crane tip trajectory in Figure 6. "FB" denotes the feedback signal in the figures. Specifically, the knuckle cylinder retracts initially and extends after 42 s, while the main cylinder extends initially and retracts after 53 s. Both the main and knuckle cylinders closely

FIGURE 7
VCC knuckle cylinder (KC) and main cylinder (MC) position tracking performances. **(A)** KC position signals. **(B)** KC position tracking errors. **(C)** MC position signals. **(D)** MC position tracking errors.
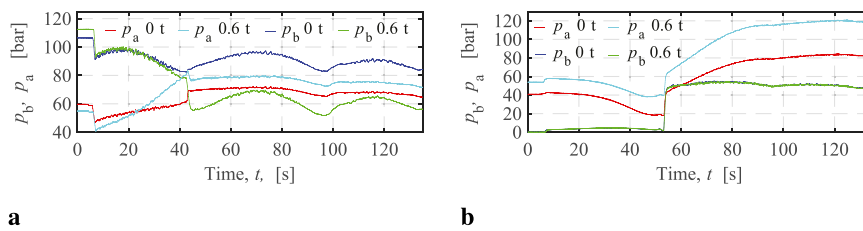
FIGURE 8
VCC KC and MC pressures. **(A)** KC bore-side and rod-side pressures. **(B)** MC bore-side and rod-side pressures.
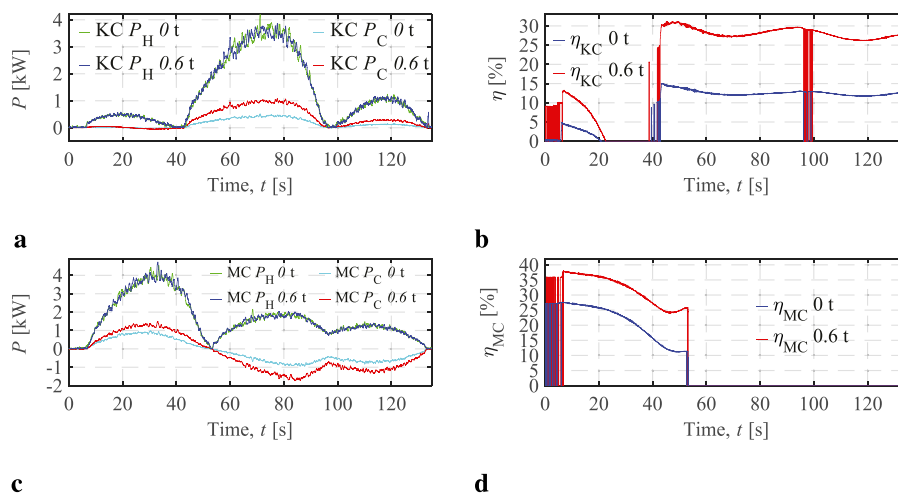
FIGURE 9
VCC KC and MC energy performances. **(A)** KC hydraulic and cylinder powers. **(B)** KC efficiencies in two load cases. **(C)** MC hydraulic and cylinder powers. **(D)** MC efficiencies in two load cases.
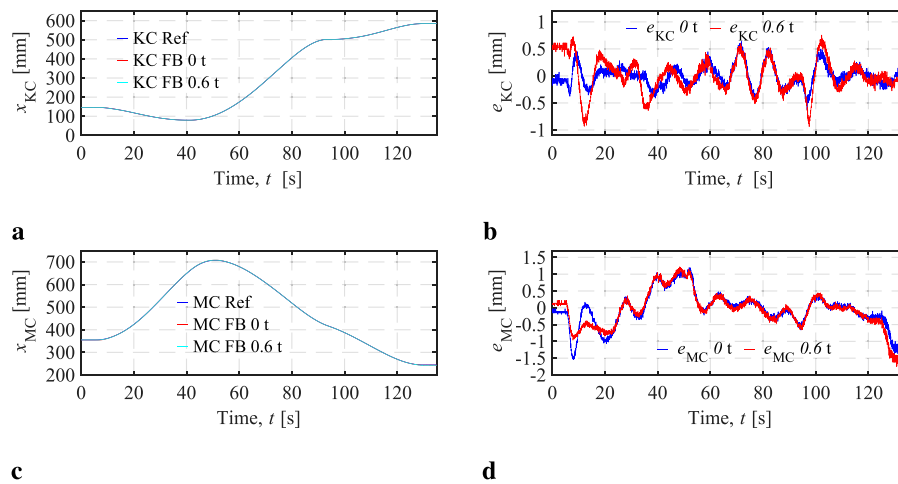
FIGURE 10
MCC KC and MC position tracking performances. **(A)** KC position signals. **(B)** KC position tracking errors. **(C)** MC position signals. **(D)** MC position tracking errors.

$$P_C = F_{cyl} \cdot v \tag{1}$$

$$F_{cyl} = p_a A_a - p_b A_b \tag{2}$$

$$P_H = p_{HPU} \cdot Q_{in} \tag{3}$$

$$Q_{in} = \begin{cases} A_a \cdot v & \text{if } v \geq 0 \\ A_b \cdot v & \text{if } v < 0 \end{cases} \tag{4}$$

$$\eta = \frac{P_C}{P_H} \cdot 100\% \tag{5}$$

It can be seen that the input powers across two load cases for both the knuckle and main cylinders are identical, assuming negligible measurement noise. This is expected since the parameters p_{HPU} and Q_{in} are independent of the applied loads. The output power of both cylinders increases with an increasing load, indicating that the cylinder efficiencies are higher under heavier loads, which is calculated using Equation 5. Specifically, the highest efficiency of the knuckle cylinder, denoted as η_{KC}, is approximately 15% with a 0 t payload and increases to about 30% with a 0.6 t payload. Similarly, the efficiency of the main cylinder, denoted as η_{MC}, is 27% with a 0 t payload and increases to 38% with a 0.6 t payload. A valve-controlled cylinder cannot regenerate energy from the payload, meaning the input power P_{in} is always positive. When the output power P_{out} is negative, efficiency η appears negative, which is irrelevant to this research. Thus, negative efficiency values are represented as zero in the plots.

It should be noted that the VCC efficiencies observed in this study are relatively high compared to typical cases described in the literature (Liang et al., 1999; Love, 2012). This discrepancy arises because the energy losses of the lab's HPU were not considered. The central HPU, which supports multiple hydraulic end users via a ring line system, consists of a pressure controlled variable-displacement pump, and a manually adjustable pressure setting of said pump. Calculating the HPU losses for the specific knuckle boom crane in this study is impractical. Therefore, the actual cylinder efficiencies, including the hydraulic power source, would likely be much lower than those observed above.

4.3 Motor-controlled crane

The position tracking performance of the two cylinders in the motor-controlled knuckle boom crane, across two load cases, is depicted in Figure 10. Both the main and knuckle cylinders exhibit precise tracking of the reference signal. The tracking error for the knuckle cylinder remains within ±1 mm, while for the main cylinder, it fluctuates between −2 mm and 1.5 mm. The MCCs demonstrate significantly better position tracking than the VCCs, primarily due to the basic control algorithm used in the VCCs. Notably, the MCC tracking errors in this study are slightly better than those reported in Hagen et al. (2019a), where the control performances of a 1M1P MCC and a VCC were thoroughly analyzed and compared.

The cylinder pressures of the motor-controlled crane are depicted in Figure 11. It is observed that the minimum pressures in both the knuckle and main cylinders are well controlled at 15 bar during crane operations, demonstrating the pressure control capability of the 2M2P MCC. The knuckle cylinder pressures increase with the increasing load. Notably, for the motor-controlled main cylinder, the bore-side and rod-side pressures never intersect, and the bore-side pressure, which drives the load, increases with the increasing load. Overall, the cylinder pressure levels in MCCs are generally lower than those in VCCs across both load cases.

The cylinder mechanical power in MCCs is also represented as P_C and calculated using Equation 1. The total shaft power of two electric servo motors (P_M) is calculated via Equations 6–8. The same method of calculation was also used in Zhao et al. (2023). T_1 and T_2 are the measured shaft torques of M_1 and M_2 from the motor drives. P_{M1} and P_{M2} are the calculated M_1 and M_2 shaft powers.

$$P_{M1} = T_1 \cdot \omega_1 \tag{6}$$

$$P_{M2} = T_2 \cdot \omega_2 \tag{7}$$
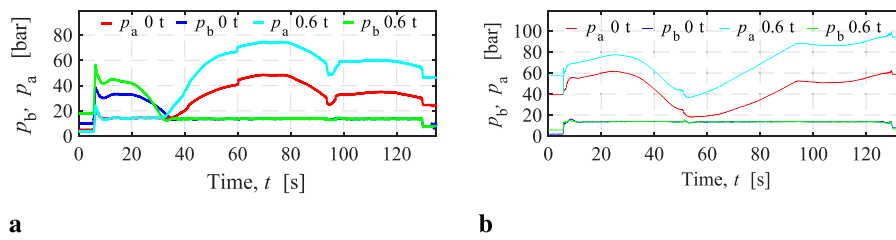
$$P_M = P_{M1} + P_{M2} \tag{8}$$

FIGURE 11
MCC KC and MC pressures. **(A)** KC bore-side and rod-side pressures. **(B)** MC bore-side and rod-side pressures.
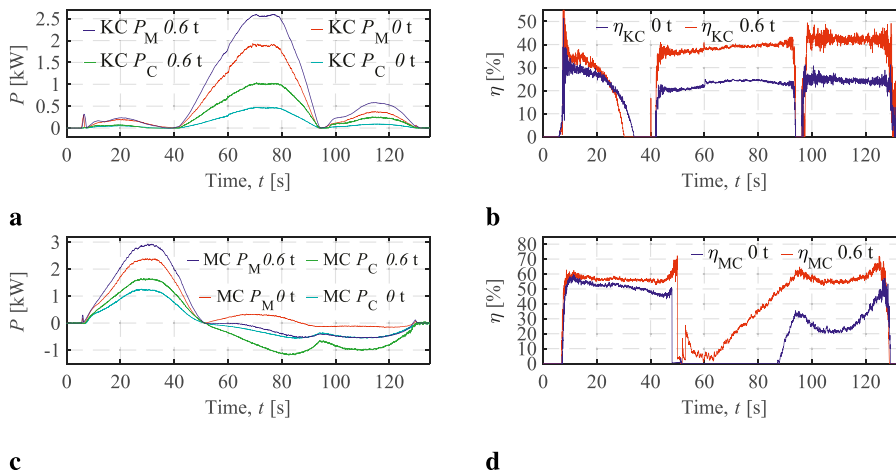

FIGURE 12
MCC KC and MC energy performances. **(A)** KC motor and cylinder powers. **(B)** KC efficiencies in the two load cases. **(C)** MC motor and cylinder powers. **(D)** MC efficiencies in two load cases.

Figure 12 illustrates the energy performances of the motor-controlled knuckle and main cylinders. As shown in Figure 12A, the input power of the motor-controlled knuckle cylinder increases with the payload. Notably, during the lifting path, the motor-controlled knuckle cylinder operates without an energy regeneration mode, and its efficiencies across the two load cases are depicted in Figure 12B. These efficiencies, calculated using Equation 5, increase from approximately 25%–40% as the payload increases.

As shown in Figure 12C, the motor-controlled main cylinder operates in two distinct modes, with a transition occurring around 50 s, where the cylinder output powers turn negative. In the energy consumption mode (positive output powers), input power increases with the payload. On the other hand, in the energy regeneration mode (negative output powers), input power decreases as the payload increases. Figure 12C illustrates the efficiencies of the motor-controlled main cylinder, which are calculated differently for each mode using Equation 9. In the third case of Equation 9, where $P_C < 0$ and $P_M > 0$, the regenerated energy from the payload is insufficient to fully compensate for the system's energy losses and the energy directed to the accumulator. Consequently, the electric servo

motor must supply additional energy to the system to enable the payload to follow the desired path.

$$\eta = \begin{cases} \dfrac{P_C}{P_M} \cdot 100\% & \text{if } P_C \geq 0 \text{ and } P_M \geq 0 \ \text{(Energy consumption)} \\[2ex] \dfrac{P_M}{P_C} \cdot 100\% & \text{if } P_C < 0 \text{ and } P_M < 0 \ \text{(Energy regeneration)} \\[2ex] 0 & \text{if } P_C < 0 \text{ and } P_M > 0 \ \text{(Pure energy loss)} \end{cases}$$

$$(9)$$

In Figure 12D, in energy consumption mode (before 50 s), the main cylinder's efficiency with a 0.6 t payload is around 60%, slightly higher than the 50% efficiency observed with a 0 t payload. In energy regeneration mode, the efficiency with a 0.6 t payload reaches approximately 60%, significantly surpassing the 30% efficiency in the 0 t payload case. It is also noteworthy that energy regeneration in the 0.6 t payload begins around 50 s, whereas in the 0 t payload, it starts only after 86 s, due to the smaller load being insufficient to overcome initial system energy losses. It is important to note that the actual regenerative efficiencies would likely be lower than those observed above. An electric power storage device is missing in the experiments and therefore, the potentially regenerative power

FIGURE 13
Total energies use by the valve-controlled crane and the motor controlled-crane.
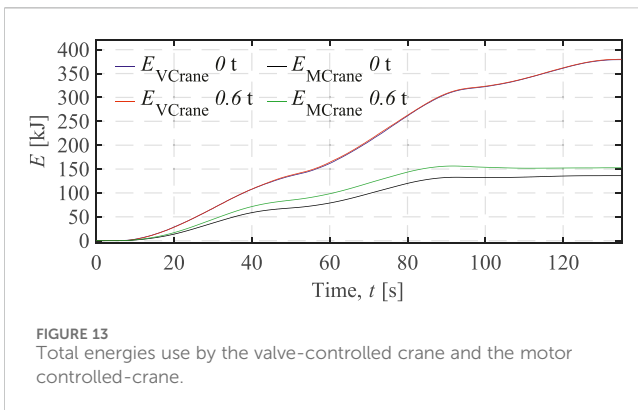
is dissipated by a resistor connected to the electric motor drive but in the analysis that power is considered 100% regenerated. It should be noted that energy flows into the accumulator during cylinder retraction and out of the accumulator during cylinder extension as the crane moves the payload along the desired path. However, since the accumulator pressure varies between 2 bar and 3 bar, these power contributions are negligible compared to P_C and P_M. As such, they are not explicitly calculated in this paper. Nevertheless, because the crane's path includes both cylinder extension and retraction phases, the energy exchanged with the accumulator is inherently accounted for in the calculation of total energy consumption.

Compared to the VCCs in the valve-controlled crane, the MCCs in the motor-controlled crane demonstrate significantly higher energy efficiencies in energy consumption mode, even though HPU losses were not considered for the VCCs. Additionally, the VCCs lack energy regeneration capability, resulting in complete system energy loss when the output is negative. Therefore, the MCCs would substantially improve the overall energy utilization compared to VCCs.

4.4 Total energy consumption in two systems

The total energy consumed by the valve-controlled (E_{VCrane}) and the motor-controlled (E_{MCrane}) knuckle boom cranes in the two load cases is shown in Figure 13. The total energy used by each crane is calculated by integrating the input powers of the knuckle and main cylinders over time, then summing the results. As shown, the valve-controlled crane consumes nearly identical amounts of total energy in both load cases, approximately 380 kJ. This is because, according to Equation 3, the hydraulic power from the central HPU remains consistent if the payload motion is unchanged. Furthermore, the total energy consumption steadily increases throughout the operation since no potential energy can be regenerated by the VCC.

For the MCCs, the total energy used increases with a greater payload. However, due to energy regeneration by the main cylinder, the total crane input energy remains almost steady at 0 t payload and decreases slightly with a 0.6 t payload after approximately 130 s. The final total energy used in the two load cases is 153 and 136 kJ, respectively. Consequently, in this study, using the motor-controlled

crane instead of the valve-controlled crane results in 60%–64% total energy savings.

5 Conclusion

This paper addresses the comparison between valve-controlled hydraulic cylinder systems and two-motor-two-pump motor-controlled hydraulic systems. This type of comprehensive comparison has been performed for a real-life application characterized by:

- A knuckle boom crane, powered either by two valve-controlled hydraulic cylinders or by two two-motor-two-pump motor-controlled hydraulic cylinders, is employed in two distinct load cases.
- A specific crane lifting path is generated within the operational range of the crane to facilitate the experiment.
- The experimental results of the two systems, including position-tracking performance, cylinder pressures, and power and energy performance, are presented, compared, and analyzed in detail.

In conclusion, the two-motor-two-pump motor-controlled hydraulic knuckle boom crane demonstrates higher efficiency and better energy regeneration capabilities compared to its valve-controlled counterpart under the two loaded test cases. These improvements lead to notably lower energy consumption for the motor-controlled crane. This research serves as an example of experimental validation, highlighting the higher energy efficiency of this innovative hydraulic technology.

Data availability statement

The raw data supporting the conclusions of this article will be made available by the authors, without undue reservation.

Author contributions

Funding

Acknowledgments

We would like to express our sincere gratitude to the following lab engineers for their invaluable assistance in building and testing the experimental setup: Jan Andreas Holm, Harald Sauvik, and Jan Christian Bjerke Strandene. Their expertise and willingness to help were instrumental in the successful completion of this project.

Conflict of interest

The authors declare that the research was conducted in the absence of any commercial or financial relationships that could be construed as a potential conflict of interest.

Generative AI statement

The author(s) declare that no Generative AI was used in the creation of this manuscript.

Publisher's note

All claims expressed in this article are solely those of the authors and do not necessarily represent those of their affiliated organizations, or those of the publisher, the editors and the reviewers. Any product that may be evaluated in this article, or claim that may be made by its manufacturer, is not guaranteed or endorsed by the publisher.

References

Ahn, K. K., Yoon, J. I., and Truong, D. Q. (2011). "Design and verification of a new energy saving electric excavator," in *In the proceedings of the 28th international symposium on automation and robotics in construction (ISARC 2011)*. Editor S. Kwon (Seoul, Korea: International Association for Automation and Robotics in Construction IAARC), 259–264. doi:10.22260/ISARC2011/0046

Cho, S. H., and Helduser, S. (2008). Robust motion control of a clamp-cylinder for energy-saving injection moulding machines. *J. Mech. Sci. Technol.* 22, 2445–2453. doi:10.1007/s12206-008-0907-6

Hagen, D., Padovani, D., and Choux, M. (2019a). A comparison study of a novel self-contained electro-hydraulic cylinder versus a conventional valve-controlled actuator-part 2: energy efficiency. *Actuators* 8, 78. doi:10.3390/ACT8040078

Hagen, D., Padovani, D., and Choux, M. (2019b). Enabling energy savings in offshore mechatronic systems by using self-contained cylinders. *Model. Identif. Control* 40, 89–108. doi:10.4173/mic.2019.2.2

Ketelsen, S., Andersen, T. O., Ebbesen, M. K., and Schmidt, L. (2020). A self-contained cylinder drive with indirectly controlled hydraulic lock. *Model. Identif. Control* 41, 185–205. doi:10.4173/mic.2020.3.4

Liang, X., Virvalo, T., and Linjama, M. (1999). "The influence of control valves on the efficiency of a hydraulic crane," in The proceedings of the Sixth Scandinavian International Conference on Fluid Power, Tampere, Finland, May 26 - 28, 1999, 381–394.

Love, L. J. (2012). Estimating the impact (energy, emissions and economics) of the us fluid power industry. *Oak Ridge Natl. Lab.* doi:10.2172/1061537

Lubecki, M., Stosiak, M., Skačkauskas, P., Karpenko, M., Deptuła, A., and Urbanowicz, K. (2022). Development of composite hydraulic actuators: a review. *Actuators* 11, 365. doi:10.3390/act11120365

Williamson, C., and Ivantysynova, M. (2008). "Pump mode prediction for four-quadrant velocity control of valueless hydraulic actuators," in The proceedings of JFPS International Symposium on Fluid Power, Toyama, Japan, 323–328. doi:10.5739/isfp.2008.323

Zhang, S., Minav, T., and Pietola, M. (2017). "Decentralized hydraulics for micro excavator," in The proceedings of the 15th Scandinavian International Conference on Fluid Power, Linköping, Sweden, 187–195. doi:10.3384/ecp17144187

Zhao, W., Bhola, M., Ebbesen, M. K., and Andersen, T. O. (2023). A novel control design for realizing passive load-holding function on a two-motor-two-pump motor-controlled hydraulic cylinder. *Model. Identif. Control* 44, 125–139. doi:10.4173/mic.2023.3.3

Zhao, W., Ebbesen, M. K., and Andersen, T. O. (2022). "Identifying the future research trend for using speed-controlled hydraulic cylinders in offshore applications through literature survey," in the proceedings of the 2022 IEEE Global Fluid Power Society PhD Symposium (presented), Naples, Italy.

Zimmerman, J. D., Pelosi, M., Williamson, C. A., and Ivantysynova, M. (2007). "Energy consumption of an ls excavator hydraulic system," in The proceedings of ASME 2007 International Mechanical Engineering Congress and Exposition, Seattle, Washington, USA, 117–126. doi:10.1115/imece2007-42267